Blind Source Separation in Retinal Videos

Eduardo S. Barriga[*a], Paul W. Truitt[b], Marios S. Pattichis[a], Dan T'so[c], Young H. Kwon[d], Randy H. Kardon[d], and Peter Soliz[b]

[a]Department of Electrical and Computer Engineering, The University of New Mexico, Albuquerque, NM 87131; [b]Kestrel Corporation, Albuquerque, NM 87109; [c]SUNY Health Science Center, Syracuse, New York; [d]Department of Ophthalmology and Visual Sciences, University of Iowa Hospital and Clinics, Iowa City, IA 52242

ABSTRACT

An optical imaging device of retina function (OID-RF) has been developed to measure changes in blood oxygen saturation due to neural activity resulting from visual stimulation of the photoreceptors in the human retina. The video data that are collected represent a mixture of the functional signal in response to the retinal activation and other signals from undetermined physiological activity. Measured changes in reflectance in response to the visual stimulus are on the order of 0.1% to 1.0% of the total reflected intensity level which makes the functional signal difficult to detect by standard methods since it is masked by the other signals that are present. In this paper, we apply principal component analysis (PCA), blind source separation (BSS), using Extended Spatial Decorrelation (ESD) and independent component analysis (ICA) using the Fast-ICA algorithm to extract the functional signal from the retinal videos. The results revealed that the functional signal in a stimulated retina can be detected through the application of some of these techniques.

Keywords: Retinal function, optical imaging, functional retinal imaging, infrared reflectance, principal component analysis, independent component analysis, blind source separation.

1. INTRODUCTION

As early as 1949, Hill and Keynes linked the activity of the nerve cells with changes in their optical properties [1]. In 1986, Grinvald et al. [2] showed that changes in the optical properties of the tissue could be used to study the functional architecture of the cortex. Villringer and Chance [3] used near-infrared light to measure non-invasively brain activity in humans through the skull. Kardon et al. [4] reported the first device to directly image the retina to record changes in 700 nm light caused by retinal activation in response to a 535 nm stimulus.

Parallel to this research in the neuroscience field, a group of algorithms for BSS has been developed in recent years [5, 6, 7, 8, 9]. In recent years, BSS and ICA have been applied to many biological related problems such as electroencephalography (EEG) data analysis [10, 11] and electrocardiogram (ECG) data analysis [12]. Stetter et al. applied BSS techniques to isolate changes on the brain cortex of a macaque monkey due to visual stimulation [13, 14, 15]. In this work, we applied BSS techniques [16] to isolate the changes produced in the retina due to visual stimulation. This research is the first to produce evidence that the functional activity in the human retina can be measured directly and non-invasively.

2. BIO-CHEMICAL BASIS FOR OPTICAL SIGNAL

Direct optical recording of the reflectance changes due to neuronal signals on the visual cortex has been demonstrated by Grinvald et al. [2]. Changes in the inherent optical properties of active brain tissue due to blood-oxygen perfusion or metabolic changes (referred to as "intrinsic signals") permit visualization of neuronal activity. The intrinsic signals are measured as a change in the percent reflectance of the illumination light occurring as a result of the change in the absorption coefficient of light at a certain wavelength due to the conversion of oxyhemoglobin to deoxyhemoglobin in response to the metabolic demands of active neurons or increases in oxyhemoglobin blood volume. The interrogating

[*]simonb@eece.unm.edu; phone 1 505 345-2327; fax 1 505 345-2649; www.kestrelcorp.com

light measures the difference in absorption spectra between the oxyhemoglobin and deoxyhemoglobin molecule in the region of 700nm.

Direct functional imaging of the human retinal has been previously reported by Kardon et al. [4]. The device that was employed for stimulating the retina and capturing functional images of the retina has been described previously by Kardon, et al. Similarly, Kardon, et al. describe a traditional approach for analyzing the video data that was based on image averaging to obtain an average state of the retina for each of the stimulus and non-stimulated periods.

The initial hypothesis was based on data collected for similar experiments where differential retinal stimulation was observed by imaging visual cortex. In these experiments Villringer [3], for example, observed a pattern in the response signal at 700 nm that appears to show an increase in the reflectance in portions of the visual cortex shortly after the onset of the stimulation to the retina. This characteristic change is consistent with an increase in oxygenated hemoglobin.

3. METHODOLOGY

3.1 Data collection

The OID-RF device applies a stimulus pattern at 530±5 nm while interrogating the oxyhemoglobin change at 700±20 nm. The stimulus pattern is applied during a 13s epoch consisting of 3s of baseline data (no stimulus), followed by 5s of continuous stimulus, and 5s of recovery time (no stimulus). During the epoch, the fundus camera captures 52 frames of 167x172 pixels in size.

3.2 Data preprocessing

In this study we present the analysis of two normal patients, M6 and M8. The data set consisted of 30 epochs for M8, with both superior and inferior retinal stimulus and 60 epochs for M6, with full field, superior and inferior retinal stimulus, with each epoch consisting of 52 image frames of data. The first step was to register all the videos using cross-correlation techniques. Next we had to determine which epochs presented unwanted artifacts, like blinks or excessive movement. To eliminate the epochs with artifacts, we calculated the standard deviation of the pixels intensity over each epoch and removed those epochs with high standard deviation. The epochs with the same stimulus condition were averaged to reduce random noise. The result was an average epoch also consisting of 52 frames. Each stimulus condition resulted in an average epoch.

The number of frames is further reduced by calculating average frames that represent blocks of time in the epoch. For example, two blocks of five frames each represent the base period; three blocks represent the stimulus period and three blocks the recovery period. Finally, to perform a First Frame Analysis [17], the first block was subtracted from the rest of the block. At this stage of the preprocessing seven images represent the time course of each stimulus condition.

3.3 Principal component analysis

The purpose of principal component analysis (PCA) is to derive a relatively small number of decorrelated linear combinations (principal components) of a set of random variables while retaining as much of the original information as possible. Using PCA the functional signal can be reconstructed using a subset of the principal components [13].

PCA can be converted to the eigenvalue problem of the covariance matrix of the data matrix [18]; hence it is solved by calculating the eigenvalues and eigenvectors of the estimated covariance matrix as in equation 1.

$$\hat{R}_{xx} = E\left\{x(k)\,x^T(k)\right\} = V\Lambda V^T \tag{1}$$

Where $\Lambda = diag\left\{\lambda_1, \lambda_2, ..., \lambda_m\right\}$ is a diagonal matrix that contains the eigenvalues and $V = \left[v_1, v_2, ..., v_m\right]$ is a matrix containing the eigenvectors. Given this, the n-th principal component can be calculated by

$$y_n = \lambda_n^{-\frac{1}{2}} v_n^T X\,. \tag{2}$$

The functional signal $\hat{X}$ can be reconstructed using a combination of the principal components, and is calculated by

$$\hat{X} = \sum_{n=n_1}^{n_2} v_n \left(v_n^T X\right) = \sum_{n=n_1}^{n_2} v_n \lambda_n^{1/2} y_n\,. \tag{3}$$

3.4 Independent component analysis

ICA is the process of estimation of all the source signals and/or the identification of a mixing matrix **H** or its pseudo-inverse separating matrix $\mathbf{W}=\mathbf{H}^{+}$ assuming only the statistical independence of the primary sources and linear independence of columns of **H** [18].

ICA has been successfully applied in many biomedical engineering problems such as separation of ECG signals [12], EEG data processing [10] and brain imaging processing [17]. There are many available algorithms for ICA [18], but for this paper we only present the results based on the fast-ICA algorithm [9].

The fast-ICA algorithm computes the demixing matrix in an adaptive fashion, computing one row at a time using the following equation:

$$w_i(j+1) = E\left(y\left(w_i^T(j)\, y \right)^3 \right) - 3w_i(j), \tag{4}$$

where $\mathbf{w_i(j+1)}$ is the i-th row for the (j+1)-th iteration and **y** is the whitened version of the data using the Karhunen-Loeve transformation.

3.5 Blind source separation

ICA makes the assumption that the sources are statistically independent. Blind source separation (BSS) tries to estimate the sources even if they are not completely statistically independent. Most ICA algorithms use higher order statistics while BSS uses only second order statistics.

In this work we use the extended spatial decorrelation (ESD) algorithm for BSS. The ESD algorithm was developed by Schiessl et al. [15] based in a second order BSS algorithm introduced by Molgedey and Schuster [7]. ESD has been used for separation of sources in optical imaging recordings [13, 14, 15].

The ESD algorithm tries to obtain the separated estimated sources by calculating the covariance matrices of the data for a good set of data and optimize the demixing matrix **W** in a way that the covariance matrix of the estimated sources is diagonal [17].

We have to solve the M(M+1) equations given by

$$C_x(0) = \sum_k H_{ik} H_{jk} C_s^{kk}(0) \tag{5}$$

$$C_x(\Delta r) = \sum_k H_{ik} H_{jk} C_s^{kk}(\Delta r) \tag{6}$$

for the M(M+1) unknowns $H_{i\neq j}, C_s^{kk}(0), C_s^{kk}(\Delta r)$. For our experiments we tried with the seven different values for Δr. It can be easily shown that due to symmetry we only need these seven values to express all the possible results (For the seven frames).

4. RESULTS

4.1 Application of principal component analysis

Applying PCA to the videos for subject M6, Figure 1 presents a set of six principal components for a specific frame, where the intensity of the principal components 2 thru 6 have been rescaled to make them visible. Calculations showed that the first principal component accounts for 95 to 98% of the information, and reproduces the general reflectance level depicted in Figure 1 (Pa1). In general it was found that the principal components 2 through 5 potentially contain the information on the functional signal, while the remaining principal components do not appear to have any useful information. One can see how the reconstructed image using the first principal component appears as a blurred version of the original video while the remaining the components present the detail.

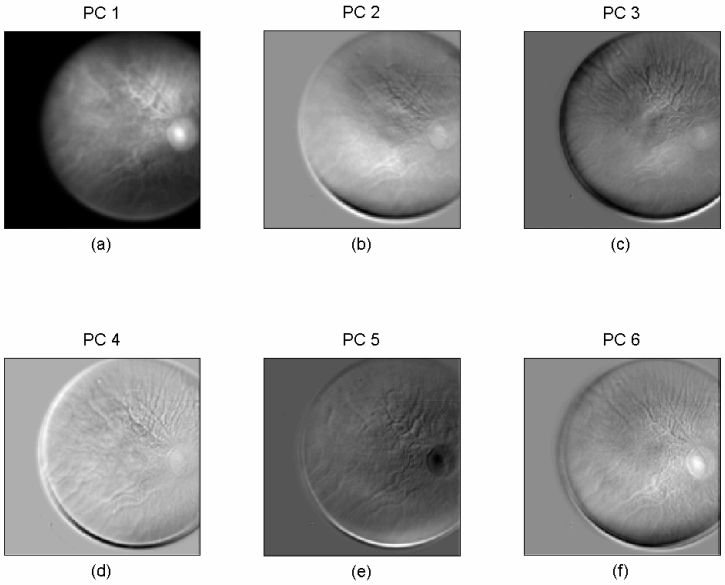

Figure 1 The set of principal components is given for subject M6 for a specific frame.

In Figure 2 the time series of the first 10 principal components (applied to the images without binning) are shown. Since the stimulus experiment consisted of 12 frames of baseline where no stimulus applied, followed by 20 frames of stimulus, the waveform that was expected was a more or less flat signal during the base and a rise in the reflectance about the 12th frame. For M6, the second principal component shows the rise in the reflectance, at about the 12th frame, which is consistent with the onset time of the stimulus. This rise in the reflectance is highly suggestive to be directly related to the functional signal.

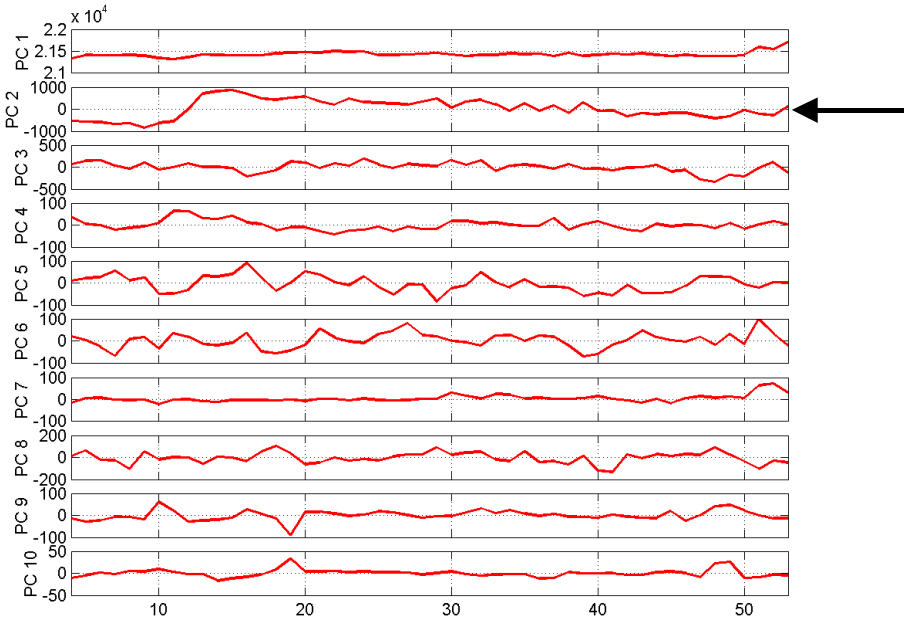

Figure 2. Time series of a set of principal components for subject M6. The arrow points to the second principal component which appears to contain the function signal.

Further analysis concentrated on the detection of a functional signal for a region of interest (ROI). The ROI's were focused on two regions of the retina, a superior and an inferior ROI, each 30x40 pixels in size. After applying first frame analysis to the images, we obtained the mean intensity value over the ROI and plotted the values through time. Figure 3 shows the ROI's intensity before and after applying PCA for the subjects M6. The two top plots are the normalized signals before PCA was applied. The expected signal is one where the stimulated region shows a rise in reflectance after "frame 1", recalling that the first data point represents the first 12 frames of the video. For M6, Figure 3, the lower two plots are after PCA. The two left plots are where the superior half of the retina was stimulated, while the two right plots are where the inferior half of the retina was stimulated.

Studying first the situation where the superior half of the retina was stimulated (left two plots), one would expect to see the solid line with square symbols to show a rise after frame #1. In both the PCA version and non-PCA version, the signal behaves as predicted. The need for PCA is demonstrated in the analysis of the right two plots where an inferior stimulus was applied. In this case the dashed line with circular symbols should show a rise at frame #2. Before the PCA was applied, the converse was observed. That is, the reflectance in the stimulated region (dashed line) decreased at frame #2 (upper right), while an increase in reflectance was observed in the unstimulated region (solid line). After PCA, the expected pattern in the reflectance signal was observed (lower right). The PCA processed signal shows a slight increase in frame #2 and continuing increase through frame #4 for the inferior region (dashed line, lower right plot). This pattern in the waveform is what is expected for an inferior stimulus.

Figure 4 shows the same four plots for subject M8. In this case the response plots for the superior stimulus (solid line) showed a decrease in reflectance at the time of the stimulus before processing with the PCA (upper left). The PCA processed signals for the superior stimulus (lower left) behaved in a manner consistent with the stimulus pattern. For the inferior stimulus, both the non-PCA and the PCA processed signals showed a pattern consistent with a inferior stimulus (dashed line). The PCA improved the saliency of the pattern (lower right, dashed line).

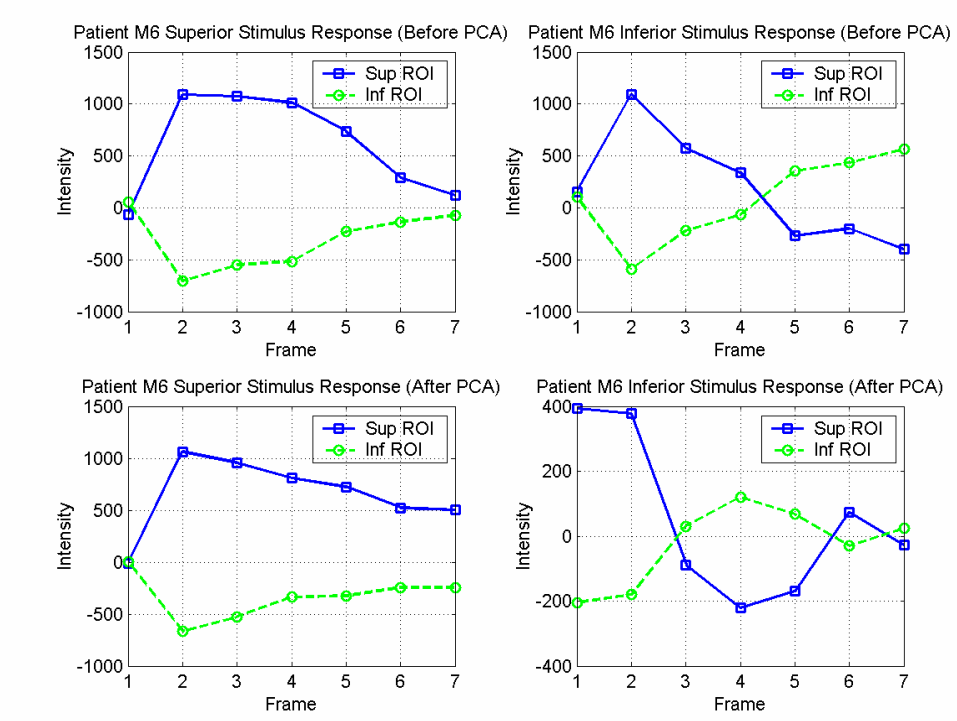

Figure 3. Intensity plots for patient M6. Top two plots represent signals before applying PCA. Bottom two plots represent the signal after applying PCA.

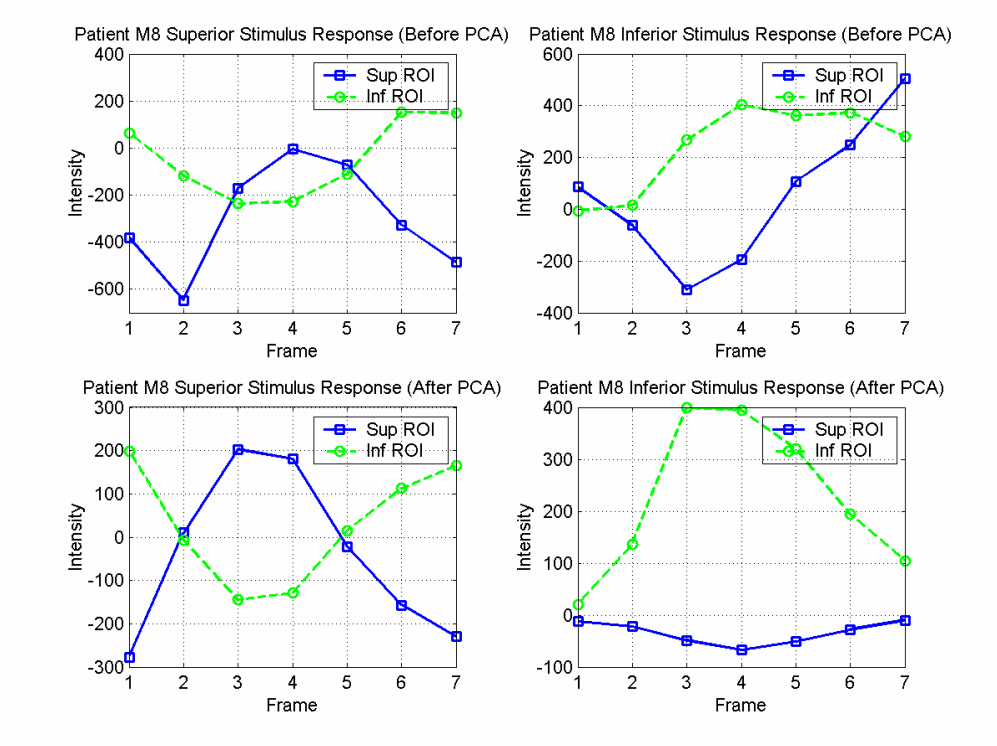

Figure 4. Intensity plots for patient M8. Top two plots represent signals before applying PCA. Bottom two plots represent signal after applying PCA.

The problem that PCA presents is that to obtain the functional signal we have to do a linear combination on the components, which is a tedious procedure and could lead us to inaccurate results. In order to solve that we used different techniques for blind source separation such as the Fast-ICA and the ESD algorithm.

4.2 Application of fast independent component analysis

In Figure 5a we see the case of an inferior stimulus for patient M6, here we can see that components 3 and 4 present a rise in the intensity of the inferior ROI after the stimulus is applied, which is the expected result. When we analyze Figure 5b we see again a rise after frame #2 in components 3 and 4, but in this case the result is not the expected because we were applying a superior stimulus and the inferior part of the retina is the one showing a rise. In this case the results are inconsistent.

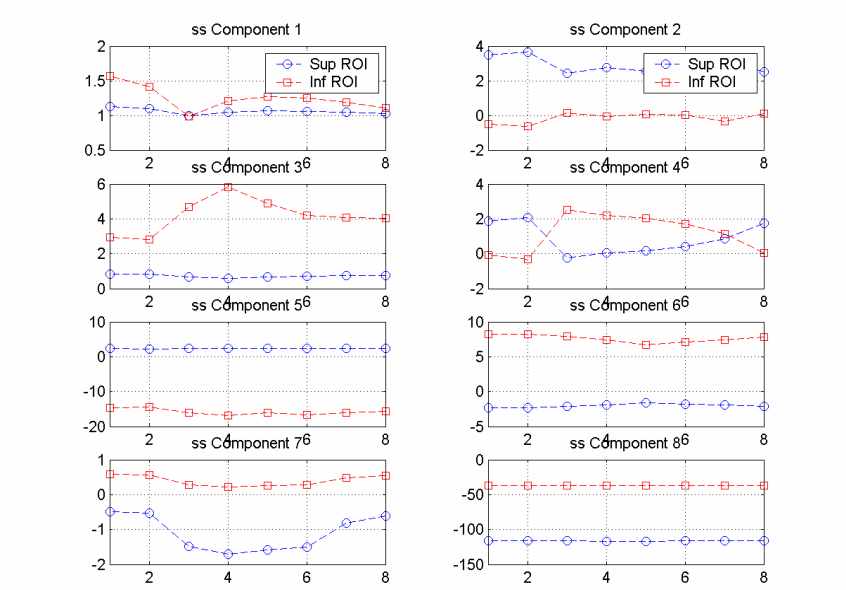

(a)

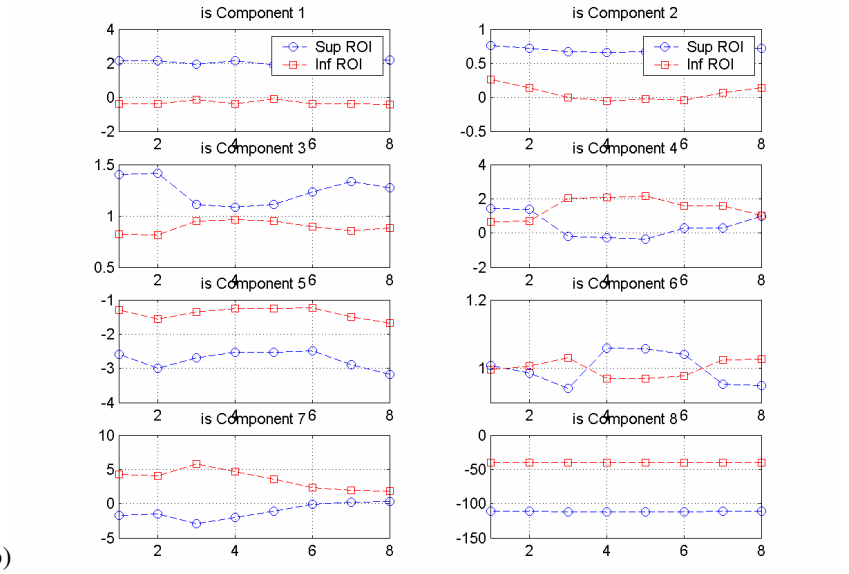

(b)

Figure 5. Results of the fast-ICA algorithm, patient M6, for (a) inferior stimulus and (b) superior stimulus.

Figure 6 shows the fast-ICA analysis for subject M8. For the superior stimulus, component 2 appears to correspond to a stimulus applied at frame 3. However, component 4 for the superior stimulus shows a pattern for the unstimulated inferior ROI that also mimics the stimulus cycle. For the inferior stimulus, there are no patterns in the inferior ROI components that are consistent with the stimulus cycle.

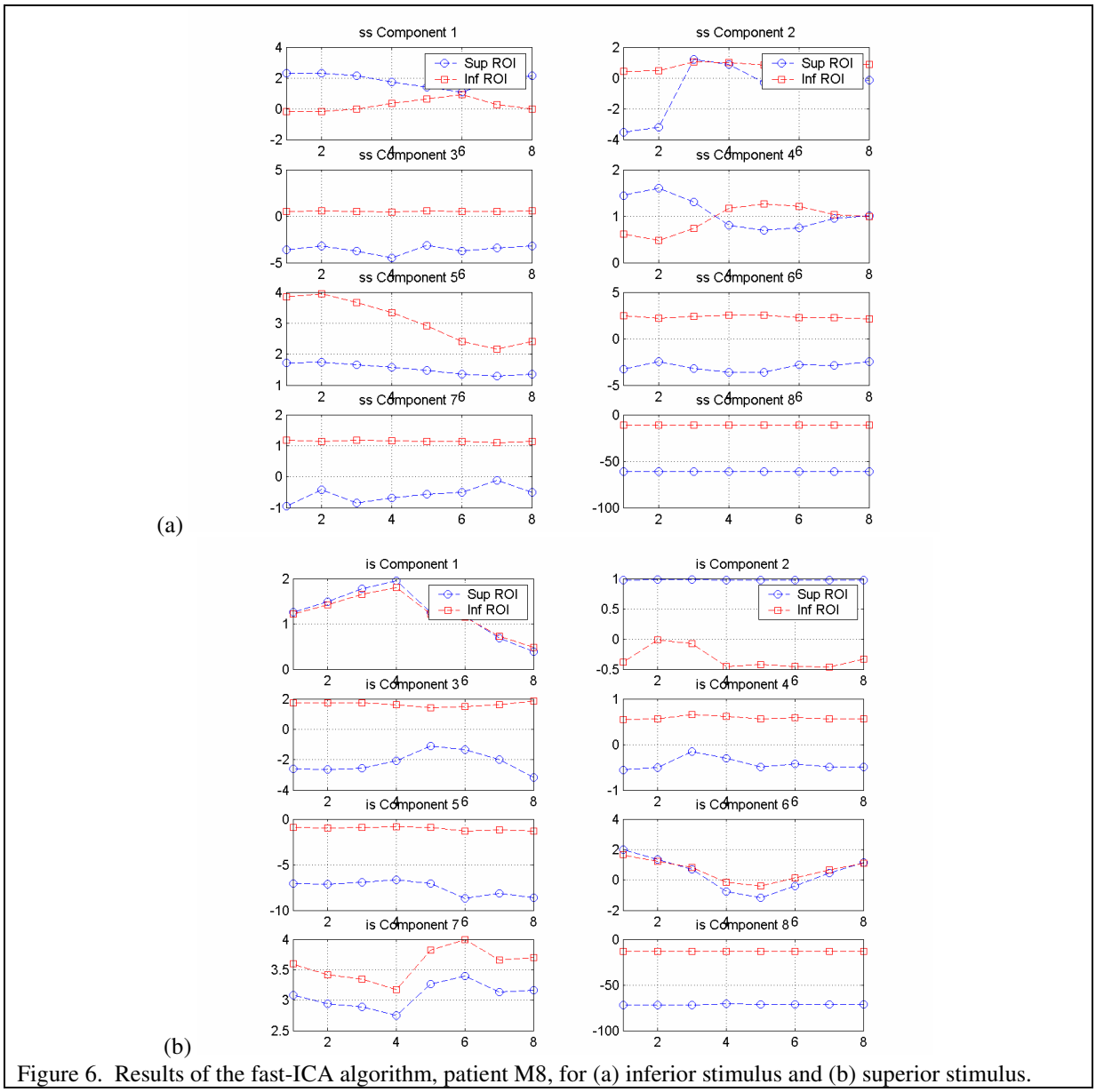

Figure 6. Results of the fast-ICA algorithm, patient M8, for (a) inferior stimulus and (b) superior stimulus.

In Figure 7 the results are presented for applying the ESD algorithm to subject M6. The results are for a lag (Δr) of 5. Figure 7a shows the response for a superior stimulus, while Figure 7b shows the response for an inferior stimulus. On the left are the responses for the superior stimulus and the right shows the responses of the inferior stimulus. In Figure 7a, the first and third components (top and bottom left) for the superior ROI and superior stimulus presents a functional response that is consistent with the stimulus cycle. In other words, the response increases for frame 3. As had been hoped, the inferior ROI responses do not correlate to the superior stimulus cycle.

Figure 7b has similarly positive results. When the stimulus is applied to the inferior ROI, the inferior ROI responds as expected, as can be seen in the first and second components (top two left side). There is no response in the unstimulated superior ROI (right) that correlates to the stimulus cycle.

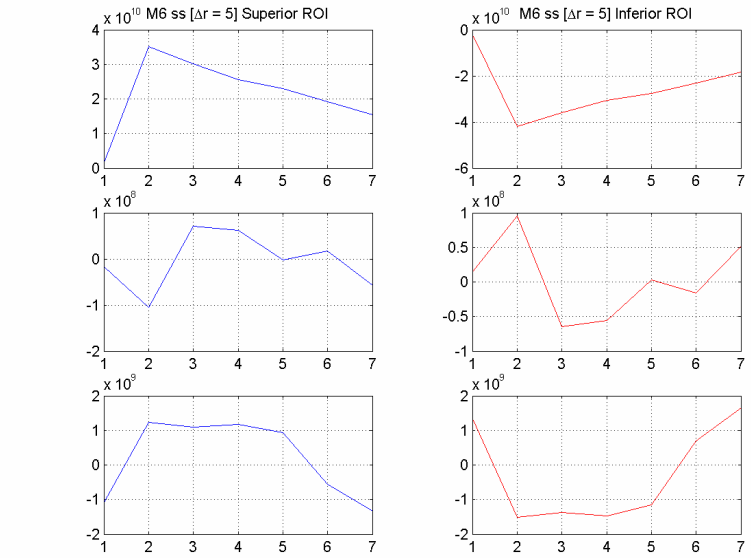

(a) Superior stimulus

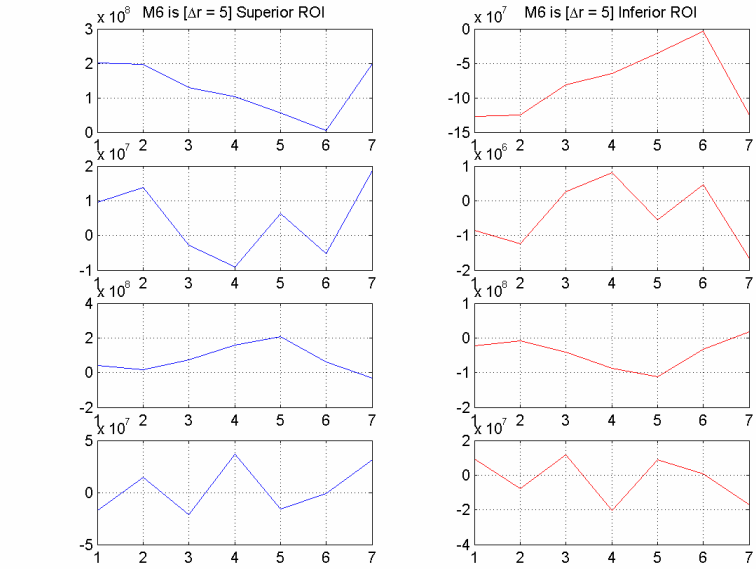

(b) Inferior stimulus

Figure 7. Results after applying the ESD algorithm, patient M6, for (a) inferior stimulus and (b) superior stimulus.

In Figure 8, the responses as processed by the BSS algorithm are plotted for subject M8. Figure 8a presents the responses for a superior stimulus. On the left of Figure 8a, the first component does indeed show a response for the superior ROI (left) that reflects the stimulus cycle, while the inferior ROI (right) does not. Figure 8b gives the responses for an inferior stimulus. On the right of Figure 8b, the first and second components of the BSS indicates a response that is consistent with the stimulus cycle.

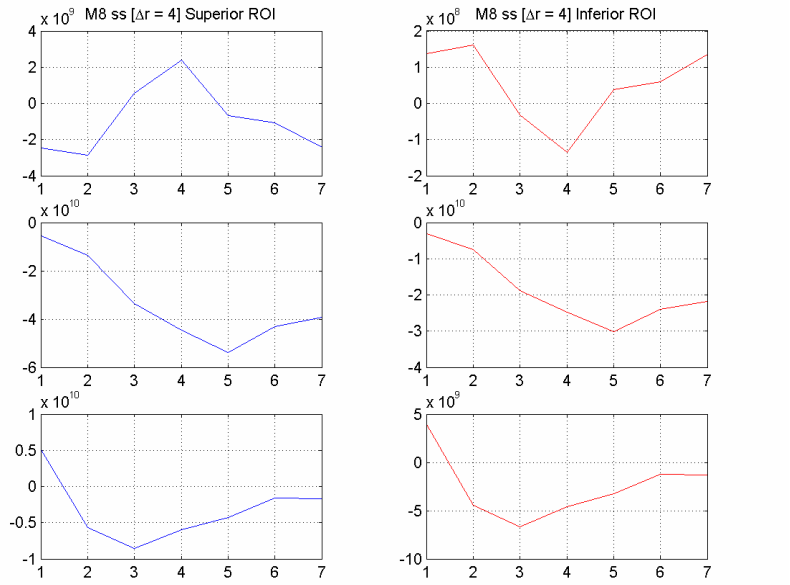

(a) Superior stimulus

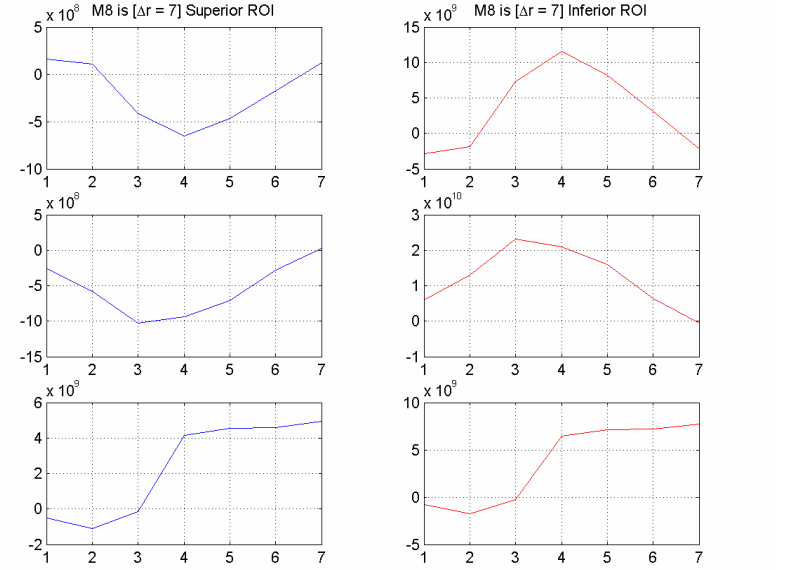

(b) Inferior stimulus

Figure 8. Results after applying the ESD algorithm, patient M8, for (a) inferior stimulus and (b) superior stimulus.

5. CONCLUSIONS

At present, the principal component(s) that appears to contain the functional signal is selected by studying the time series. This process is tedious and depends on subjective judgment, which makes it susceptible to error. Further efforts will be dedicated towards the automation of this process. Even though the fast-ICA algorithm has been proven to work in similar problems, in our case it gives us contradictory results. The reason is likely to be related to the contrast function chosen for this study and the fact that other physiological signals may be present and are correlated to the functional signal. Experimentation with the parameters of the algorithm will be performed to find the functional signal. So far, the ESD algorithm is giving the best results for finding the functional signal. The problem of the correct lag for the algorithm is yet to be solved but the results are promising.

From the results presented here, the separation of the functional signal from the other signals present appears to be promising, and further research will focused in trying to find the most suitable BSS algorithm for this problem.

ACKNOWLEDGMENTS

This research was funded under a grant from the National Eye Institute, Grant # 2R44 EY12915-02.

REFERENCES

1. Hill, D.K. and Keynes, R.D. J. *Physiol., Lond.* 108, pp 278-281, 1949.
2. Grinvald, A., Lieke, E., Frostig, R.D., Gilbert, C.D. and Wiesel, T.N., "Functional architecture of cortex revealed by optical imaging of intrinsic signals," *Letters to nature*, vol. 324, pp 361-364, November 1986.
3. Villringer, A. and Chance, B., "Noninvasive optical spectroscopy and imaging of human brain function," *Trends in Neuroscience* 20, 435-442 (1997).
4. Kardon, R., Kwon, Y.H., Truitt, P.W., Nemeth, S.C., T'so, D. and Soliz, P., "Optical imaging device of retinal function," *SPIE Photonics West*, 2002. San Jose, CA.
5. Bell, A.J. and Sejnowski, T.J., "An information-maximization approach to blind separation and blind deconvolution," *Neural Comput.*, vol 7, no. 6, pp. 1003-1034, 1995.
6. Cardoso, J., "Infomax and maximum likelihood for blind source separation," *IEEE Signal Processing Letters*, vol. 4, no. 4, April 1997.
7. Molgedey, L. and Schuster, H.G., "Separation of a mixture of independent signals using time delayed decorrelations," *Physical Review Letters*, vol. 72, no. 23, June 1994.
8. Belouchrani, A., Abed-Meraim, K., Cardoso, J., Moulines, E., "A blind source separation technique using second-order statistics," *IEEE Transactions on Signal Processing*, vol. 45, no. 2, February 1997.
9. Hyvarinen, A. and Oja, E., "A fast fixed point algorithm for independent component analysis," *Neural Comput.*, vol. 9, pp. 1483-1492, 1997.
10. Makeig, S., Bell, A.J., Jung, T.-P. and Sejnowski, T.J., "Independent component analysis of electroencephalographic data," in *Advances in Neural Information Processing Systems*, MIT Press, Cambridge MA, pp. 145-151, 1996.
11. Jung, T.-P., Humpries, C., Lee, T.-W., McKeown, M.J., Iragui, V., Makeig, S. and Sejnowski, T.J., "Removing electroencephalographic artifacts by blind source separation," *Psychophysiology*, vol. 37, pp. 163-178, 2000.
12. Choi, S., Cichocki, A. and Amari, S., "Fetal electrocardiogram data analysis via flexible independent component analysis," in *The 4-th Asia-Pacific Conference on Medical & Biological Engineering (APCMBE'99)*, Seoul, Korea, 1999.
13. Stetter, M., Schießl, I., Otto, T., Sengpiel, F., Hübener, M., Bonhoeffer, T. and Obermayer, K., "Principal Component Analysis and Blind Separation of Sources for Optical Imaging of Intrinsic Signals". *NeuroImage,* vol. 11, pp. 482-490, 2000.
14. Schiessl, I., Schoner, H., Stetter, M., Dima, A. and Obermayer, K. "Regularized second order source separation," in *Proceedings of the Second International Workshop on Independent Component Analysis and Blind Signal Separation*, Helsinki, Finland, Vol. 2, pp. 111-116, 2000.
15. Schiessl, I., Stetter, M., Mayhew, J.E. W., McLoughlin, N., Lund, J.S. and Obermayer, K. "Blind signal separation from optical imaging recordings with extended spatial decorrelation," *IEEE Transactions on Biomedical Engineering*, vol. 47: pp. 573-577, May 2000.
16. Barriga, E.S., Soliz, P. and Truitt, P.W., "Functional signal detection in retinal videos," in *The 45-th IEEE International Midwest Symposium on Circuits and Systems (MWSCAS-2002)*, Tulsa, Oklahoma, 2002.
17. Schiessl, I., "Blind source separation algorithms for the analysis of optical imaging experiments," *PhD Thesis*, Technical University Berlin, Germany, 2001.
18. Cichocki, A., Amari, S., "Adaptive blind signal and image processing," John Wiley, New York, 2002.